THE JOURNAL OF PHYSICAL CHEMISTRY C

ARTICLE

pubs.acs.org/JPCC

Hierarchical Cu_2ZnSnS_4 Particles for a Low-Cost Solar Cell: Morphology Control and Growth Mechanism

Yan-Li Zhou, Wen-Hui Zhou,* Mei Li, Yan-Fang Du, and Si-Xin Wu*

The Key Laboratory for Special Functional Materials of MOE, Henan University, Kaifeng, P.R. China, 475004

Supporting Information

ABSTRACT: In this paper, novel hierarchical Cu_2ZnSnS_4 (CZTS) particles were synthesized by a solvothermal method. The effects of synthetic conditions, such as reaction temperature, reaction time, solution concentration, and the amount of PVP, were investigated. The results showed that the size and morphology of the CZTS particles can be controlled by changing the reaction conditions and that PVP played an important role in the formation of the final hierarchical particles. Time-dependent results showed that the nucleation and growth of the CZTS particles were governed by a nucleation−dissolution−recrystallization growth mechanism. The optical and electrical properties of the CZTS particles were also investigated. Compared with spherelike CZTS particles and CZTS nanocrystals, the absorption of typical hierarchical CZTS particles decayed more slowly, indicating a higher absorption coefficient in the visible region. Meanwhile, the current−voltage characteristics of the CZTS films indicated that flowerlike particles favored the electronic transmission and thus may induce the generation of photocurrent. Thus, the obtained hierarchical CZTS particles are more suitable for using as an absorber layer in low-cost solar cells.

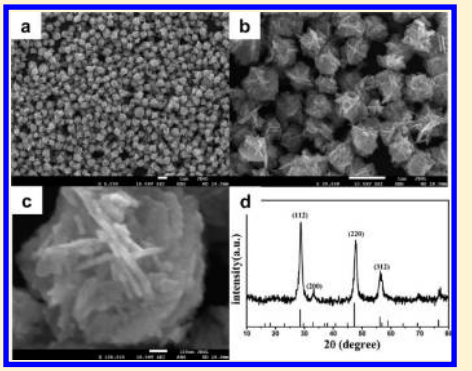

1. INTRODUCTION

During the last decades, there was an increasing interest in thin film photovoltaics due to the energy requirements and low production costs.[1] $CuInS_2$ and $CuInSe_2$ (CIS) are of considerable interest in thin-film photovoltaic devices for their high absorption coefficients and adjustable band gaps. CIGS, CIS doped with Ga, has become one of the most successful materials currently being commercialized for thin-film photovoltaic devices, and the current power conversion efficiencies of CIGS-based solar cells have been pushed beyond 20%.[2] However, indium and gallium used for preparation of the active layers are rare and expensive elements. This could lead to a shortage in the supply of these elements and would inhibit a cost-effective large-scale production.[3] So, high-quality semiconductor consisting of abundant elements with low toxicity is a good alternative for large-scale commercial applications.[4] Cu_2ZnSnS_4 (CZTS) is a quaternary semiconductor derived from CIS by replacing In(III) with Zn(II) and Sn(IV) in the ratio 50:50. It is a direct band gap semiconductor with high absorption coefficient in the visible region (over 10^4 cm^{-1}). The band gap is about 1.4−1.6 eV, which is very close to the optimum value for being used as an absorber layer in solar cells.[5,6] Moreover, it is nontoxic, and the elements are abundant in the crust of the earth in comparison with those of CIGS. Owing to these special properties, CZTS is considered to be a promising material for application in low cost and environmentally friendly thin film solar cells.[5]

Nakayama et al. had first successfully prepared stannite CZTS thin film by the spray pyrolysis method,[7] and solar cells based on CZTS have achieved power conversion efficiency as high as 6.77% under AM1.5G illumination by Rf magnetron sputtering.[8] Recently, the CZTS nanocrystals have been prepared by solution-based synthesis.[9−13] Emerging CZTS-based thin-film solar cells made in the laboratory have achieved a power conversion efficiency of up to 9.6%.[14] However, Shockley−Queisser photon balance calculations show that the theoretical limit for CZTS is 32.2%,[15] and recombination, optical, and collection losses were considered as the main limiting factors on the efficiency of chalcopyrite solar cells.[16]

Lately, self-assembled 3D hierarchical structures have been extensively studied due to their potential applications in various nanodevices.[17,18] Hierarchical nanowire has been applied to the photoelectrodes of dye-sensitized solar cells (DSCs) and the special hierarchical structure is expected to improve photoelectric transformation efficiency of thin-film solar cells.[19] The hierarchical structures not only provide a large surface area but also present extra functions, such as (1) generating light scattering and (2) strengthening electron transport. Therefore, the hierarchical structure is more suitable for a high-efficiency, yet low-cost, solar cell compared to the nanocrystals film.[20]

Herein, we demonstrated the synthesis of flowerlike CZTS particles with hierarchical structure by the simple solvothermal method. The obtained flowerlike CZTS particles were self-assembled as nanosheets, and each nanosheet had an average thickness of ∼25 nm and size of ∼500 nm. Then factors influencing the

Received: July 14, 2011
Revised: September 7, 2011
Published: September 09, 2011

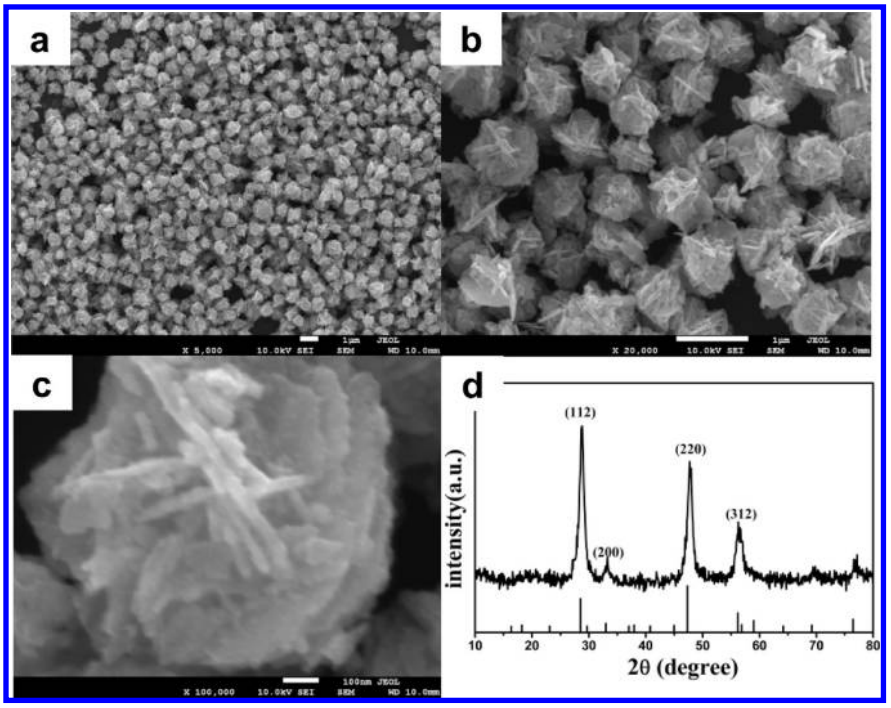

Figure 1. (a) Low-magnification and (b) enlarged FESEM images of the flowerlike CZTS particles, (b) enlarged FESEM image of the flowerlike CZTS particles (the scale bar is 1 μm), (c) FESEM image of an individual flowerlike CZTS particle (the scale bar is 100 nm), and (d) XRD pattern of the as-synthesized flowerlike CZTS particles.

morphology and size of the CZTS particles were discussed. The results showed that the size and morphology of the CZTS particles can be controlled by changing the reaction conditions and that PVP played an important role in the formation of the final hierarchical nanoparticles. In addition, the hierarchical flowerlike CZTS particles exhibited broad absorption in the visible region, and the corresponding device showed significant surface photovoltage effect between 300 and 600 nm. Due to the special morphologies and sizes, the flowerlike CZTS film exhibited the lowest electrical resistivity among three CZTS films. All the results indicated that the hierarchical CZTS nanostructure may favor the generation of photocurrent and electronic transmission. So, the hierarchical CZTS nanostructure may have great potential to be applied in high-efficiency, yet low-cost photovoltaic areas.

2. EXPERIMENTAL SECTION

2.1. Materials. Ethylene alcohol (EG), copper(II) chloride dihydrate ($CuCl_2 \cdot 2H_2O$), zinc(II) chloride ($ZnCl_2$), and tin(IV) chloride pentahydrate ($SnCl_4 \cdot 5H_2O$) were all of analytical grade and used as received. Polyvinylpyrrolidone (PVP), thiourea (CH_4N_2S), and 1-dodecanethiol (DDT) were the products of Alfa. All water used was obtained from a Milli-Q purification system.

2.2. Synthesis. In a typical experimental procedure, 0.5 mmol of copper(II) chloride dihydrate, 0.25 mmol of zinc(II) chloride, 0.25 mmol of tin(IV) chloride pentahydrate, 1.25 mmol of thiourea, and 0.45 g of PVP were dissolved in 40 mL of ethylene glycol under magnetic stirring. Then the mixture was loaded into a Teflon-lined stainless steel autoclave of 50 mL capacity. The sealed autoclave was maintained at 230 °C for 24 h and then allowed to cool to room temperature. The precipitate was centrifuged and washed with deionized water and ethanol several times to remove byproduct. The final product was vacuum-dried at 60 °C before characterization.

2.3. Characterization. The morphology and composition of the as-prepared products were characterized by field-emission scanning electron microscopy (FESEM, JSM-7001F) at an acceleration voltage of 20.0 kV and with energy dispersive X-ray spectroscopy (EDS). Transmission electron microscopy (TEM) and high-resolution TEM observations were carried out on a JSM-2010 with an emission voltage of 200 kV. The phase and the crystallographic structure of the products were identified by X-ray diffraction (XRD, Philips X′ Pert Pro, Cu Kα, λ = 0.154 056 nm). Raman spectra were obtained by a confocal microscopic Raman spectrometer (Renishaw, RM-1000). UV−vis spectroscopy (Lambda 35, PerkinElmer) was used to measure the UV−vis absorption. $I-V$ curves were measured by a semiconductor characteristic measurement system (Model SCS/F′-4200).

3. RESULTS AND DISCUSSION

3.1. Synthesis of Flowerlike CZTS Particles. The morphology and size of the as-prepared CZTS particles were shown in Figure 1a−c. From the SEM images of the sample, we can see that the product was composed of nearly dispersed flowerlike particles with hierarchical structure, and the size of the obtained particles was about 500 nm in diameter. As shown in Figure 1c, the magnified image of an individual CZTS particle indicated that the flowerlike particle was composed of nanosheets with a thickness of about 20 nm, and several nanosheets connected with each other to form the hierarchical flowerlike particle. The elemental analysis result of the typically synthetic CZTS particles performed by energy dispersive X-ray spectroscopy are shown in Figure S1 (Supporting Information). The atomic ratio

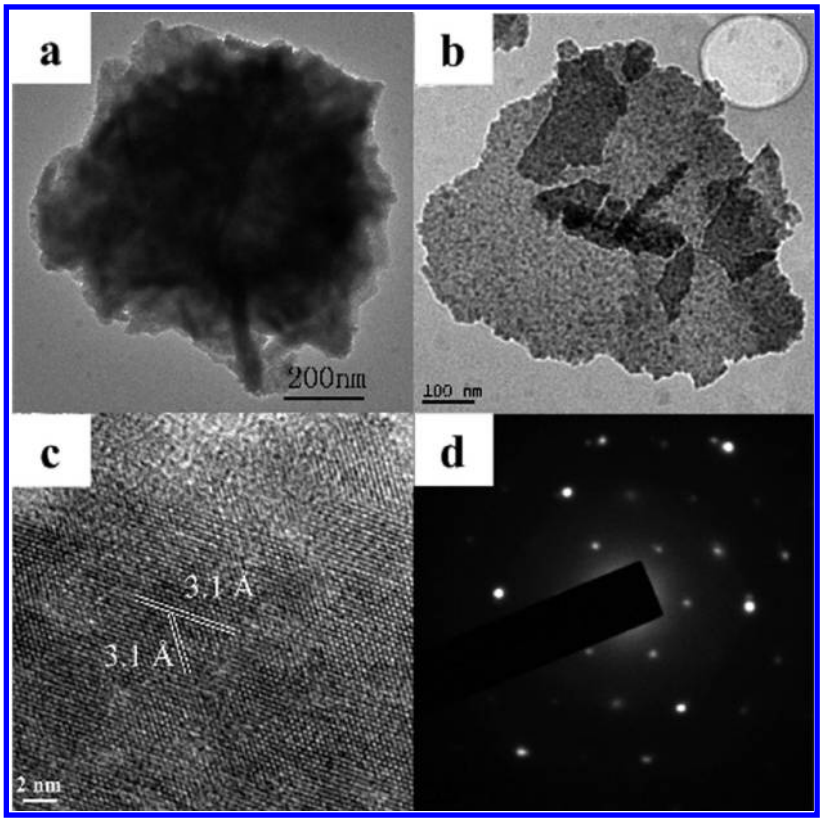

Figure 2. (a) TEM image of a single flowerlike CZTS particle, (b) magnification of a simple nanosheet, and (c) HRTEM image and (d) SAED pattern of the nanosheet.

of Cu:Zn:Sn:S was determined to be 2.10:0.80:0.96:4.00. Considering the error of the EDS detector (approximately ±2 atom %), this value basically agreed with the theoretical value of 2:1:1:4. The slightly Cu-rich and Zn-poor composition deviated from stoichiometric CZTS may be due to the difference of the reactivity and ionic radius of metal precursors. The XRD pattern of the typical sample prepared at 230 °C for 24 h is shown in Figure 1d. The diffraction peaks of as-synthesized CZTS can be indexed to pure phase of CZTS (JCPDS No. 26-0575). The major XRD diffraction peaks appeared at 2θ = 28.52°, 33.08°, 47.64°, and 56.60° attributed to (112), (200), (220), and (312) planes can be seen clearly. No obvious peaks resulting from impurities were observed, indicating the high purity of the as-synthesized CZTS. The lattice parameters ($a = b$ = 5.396 Å; c = 10.834 Å) of the typical sample refined by the Jade 5 software were similar to that described in the literature[11] ($a = b$ = 5.427Å, c = 10.848 Å). The difference may be because of the peak shift during the measurement process. The morphology of the as-synthesized CZTS particles was also investigated by TEM and HRTEM imaging. As shown in Figure 2, the particles size was about 500 nm, and some nanosheets were seen at the edge of the particles. We supposed that the flowerlike CZTS particles consisted of nanosheets. The corresponding HRTEM image showed the good crystallinity of the nanosheet. The selected area electron diffraction (SAED) pattern of the nanosheet suggested that the nanosheet was a single crystal, and thus the CZTS particles had good crystallinity. The lattice fringe with an interplanar spacing of 3.1 Å was ascribed to the (112) plane of CZTS nanoparticles. This result indicated that the nanosheets grew along the [112] direction. As seen from the XRD pattern of as-prepared CZTS, the peak intensity of (112) was stronger than that of (220), revealing that the (112) was the preferred growth plane compared to the standard XRD pattern of CZTS.

In order to study the composition of the final flowerlike particles, Raman and EDS mapping technologies were used to confirm the composition of flowerlike particles by only CZTS. Though the XRD pattern of the as-prepared CZTS particles is very similar to those of ZnS (JCPDS, Card no. 01-0792 and 05-0566) and Cu_3SnS_4 (JCPDS, Card no. 33−0501), the Raman spectrum confirmed the composition of final flowerlike particles by only CZTS (shown in Figure S2, Supporting Information). The existence of CZTS was confirmed by the intense peak at 333 cm^{-1} and the weak peak at 284 cm^{-1}, which were the characteristic peaks of CZTS and close to the reported values.[21] No other characteristic peaks of impurities were observed, such as $Cu_{2-x}S$ (475 cm^{-1}), ZnS (351 and 274 cm^{-1}), Cu_3SnS_4 (318, 348, and 295 cm^{-1}), and so on. In addition, the EDS mapping result could also confirm the composition of flowerlike particles by only CZTS (shown in Figure S3, Supporting Information). As we can see, Cu, Zn, Sn, and S are evenly distributed among the single flowerlike particle, and there is no noticeable compositional distribution among the flowerlike particle. These results excluded the presence of other binary or ternary compounds and confirmed the composition of flowerlike particles by only CZTS.

3.2. Influence of the Reaction Conditions. To ascertain the growth mechanism, we performed a number of experiments under different conditions, including adjusting of the reaction temperature (190−250 °C), reaction time (0.5−24 h), the

Table 1. Effects of the Different Reaction Conditions on the Morphologies of Resulting CZTS Products

influencing factor		morphologies	particle size	
temp/°C	190	flowerlike particles and nanosheets	500 nm	
	210	flowerlike particles and nanosheets	500 nm	
	230	flowerlike particles	500 nm	
	250	nanosheets	500 nm	
concn[a]	$1/2C_0$	flowerlike particles	3 μm	
	C_0	flowerlike particles	500 nm	
	$2C_0$	spherelike particles with rough surface	200 nm	
	$4C_0$	spherelike particles with rough surface	100 nm	
PVP/g	0	nanoparticles aggregation	no statistics	
	0.2	flowerlike particles and nanosheets	1 μm	
	0.45	flowerlike particles	500 nm	
	0.9	spherelike particles	50 nm	
time/h	0.5	spherelike particles aggregation	50 nm	
	2	spherelike particles and nanosheets	20 nm	100−300 nm
	6	nanosheets and underdeveloped nanosheets	500 nm	
	24	self-assembly of flowerlike particles	500 nm	

[a] The concentration C_0 is the typical sample.

concentration (0.5−4-fold), and the amount of PVP (0−0.9 g), and the influences of the reaction conditions on the morphologies and sizes of the as-synthesized CZTS particles are summarized in Table 1.

3.2.1. Influence of the Reaction Temperature. The XRD patterns of the samples prepared at different temperatures (190−250 °C) for 24 h showed that the diffraction peaks of all samples can be indexed to pure phase of CZTS (JCPDS No. 26-0575) (Figure S4, Supporting Information). The intensity of the diffraction peaks increased gradually with the increase of the reaction temperature, indicating the improvement of the crystallinity. The intensity of the (112) preferred orientation at 230 °C was stronger than other CZTS particles prepared at other temperatures, which means that the best crystallinity of CZTS particles was obtained at 230 °C during the solvothermal process. The morphologies and sizes of the as-synthesized CZTS particles at different temperatures are presented in Table 1. The particle size was maintained at about 500 nm when the reaction temperatures varied from 190 to 250 °C. Only at 230 °C were the uniform and nearly dispersed flowerlike particles obtained. Therefore, a temperature of 230 °C was required to obtain the typical hierarchical CZTS nanoparticles.

3.2.2. Influence of the Concentration. The influence of the concentration of the precursors in the range between $1/2C_0$ and $4C_0$ was studied. As shown in Figure 3, the concentration of the precursors had great influence on the morphology and size of the CZTS particles. When the concentration of the precursors varied from $1/2C_0$ to $4C_0$, the obtained CZTS particles changed from flowerlike particles to spherelike particles, while the particle size decreased from about 3 μm to 100 nm. As shown in Figure 3a,b, both CZTS particles prepared at high concentrations ($2C_0$ and $4C_0$) were spherelike particles with rough surface, and the sizes of obtained spherelike CZTS particles were about 200 and 100 nm, respectively. When the concentration was decreased to half of the typical value, the dominant products were flowerlike CZTS particles self-assembled by nanosheets, and the average size was about 3 μm (Figure 3d). By increasing the concentration of the precursors, the crystal size gradually decreased from approximately 10 to 7 nm (Figure 3e), this phenomenon may be explained by a kinetics mechanism. Interestingly, a gradual change of crystalline state from polycrystal to single crystal was also observed with decreasing the concentration of the precursors, but the reason is as yet unknown.

3.2.3. Influence of PVP. As an important surface ligand, PVP was expected to have great effect on the nucleation and growth of the final CZTS nanoparticles. So CZTS nanoparticles were prepared in the presence of different amounts of PVP to investigate the influence of PVP on the formation of final nanoparticles. The XRD patterns of the CZTS nanoparticles prepared with different amounts of PVP are shown in Figure S5 (Supporting Information). The XRD patterns clearly revealed that all diffraction peaks matched well with the pure phase of CZTS, and no obvious peaks resulting from impurities were observed. As the amounts of PVP increased, the major diffraction peaks of CZTS nanoparticles became narrow and sharp. The grain sizes of different CZTS nanoparticles prepared with different amounts of PVP estimated by XRD patterns are summarized in Table S1 (Supporting Information). As a general trend, the grain size decreased slightly as amounts of PVP increased. In the region of 0.20−0.45 g of PVP, the crystal size remained at almost constant value. When the amount of PVP was 0.9 g, the crystal size of CZTS particles decreased to 6.7 nm. The morphologies of the CZTS nanoparticles prepared with different amounts of PVP are shown in Figures S6 and S7 (Supporting Information). When the amount of PVP was reduced to 0.2 g, both nanosheets and quasispheres composed of the nanosheets with size 1 μm appeared in the product. When the PVP amount was increased to 0.9 g, only spherelike particles with the average diameter 100 nm were obtained. The above results demonstrated that too much PVP is not favorable for the growth of particles. At a high concentration, PVP might form a colloid to wrap the entire surface of CZTS particles, inhibiting the growth of all the directions,[22] while at a relatively low concentration, the PVP could not be completely absorbed on all the crystal planes. PVP may preferentially be absorbed on the face with a higher density of surface atoms, and the growth along this face could be considerably restricted.[23] In our experiment, 2D CZTS nanosheets may preferentially grow along the [112] direction

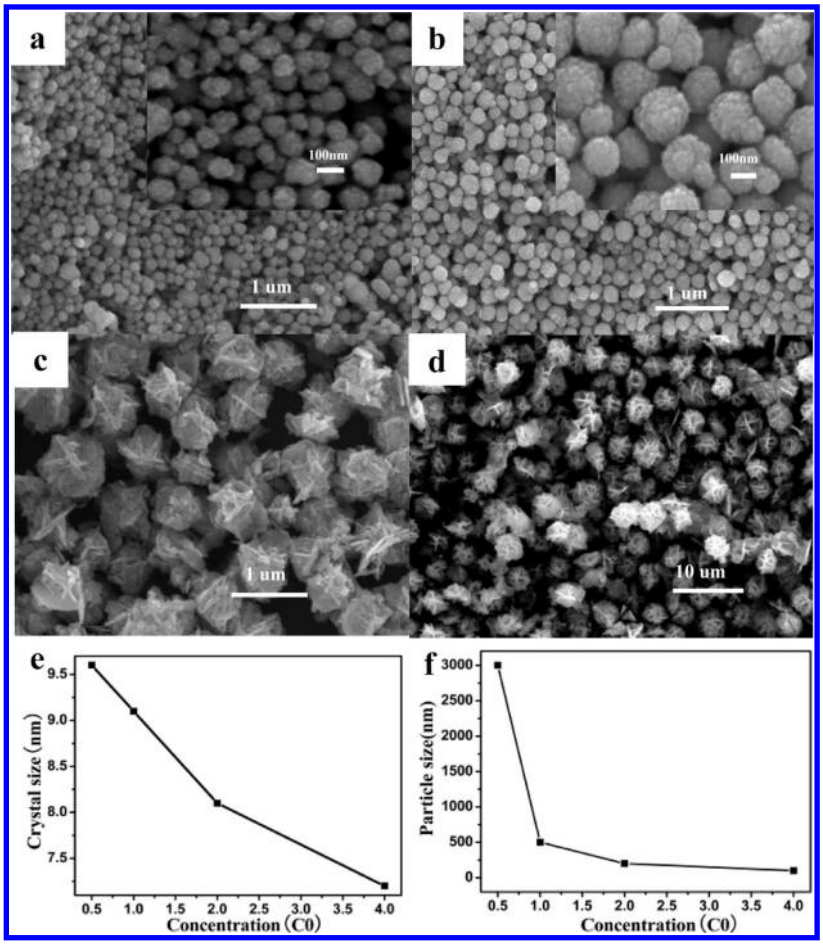

Figure 3. FESEM images of the flowerlike CZTS particles prepared at 230 °C for 24 h with different concentrations of precursors (a, $4C_0$; b, $2C_0$; c, C_0; d, $1/2C_0$). The crystal size (e) and particle size (f) as a function of precursor concentration for the CZTS particles.

and then the 2D CZTS nanosheets assembled to 3D hierarchical particles. As shown in Figure S6 (Supporting Information), when there was no PVP added to the reaction mixture, only spherelike particle agglomerates were obtained, which indicated that PVP played an important role in the growing process of flowerlike CZTS particles. In our experiments, PVP might play two main roles in the process: one is to prevent the aggregation of CZTS nanoparticles by steric hindrance during the initial growth stage; another is selective adsorption on some certain facets of CZTS crystals and the kinetic control of growth rates of these facets.[24]

3.3. Growth Mechanism. In order to further understand the growth mechanism of CZTS nanoparticles, detailed time-dependent evolution of morphology was studied by FESEM, which is shown in Figure 4. When the solvothermal reaction proceeded for 0.5 h, the dominant product was spherelike particle agglomerates. After reaction for 2 h, numerous small nanosheets were formed, and also some tiny nanocrystals were observed. When the reaction time was increased to 6 h, two-dimensional nanosheets with an average diameter of 500 nm and thickness of 20 nm appeared in the product; meanwhile, the tiny nanocrystals disappeared. Upon gradual evolution of the CZTS nanostructures, well-defined 3D flowerlike particles with irregular shape were produced after a reaction time of 24 h. As shown in Figure 4d, no other impurity shape could be observed except for flowerlike particles. On the basis of the results above, we proposed the possible growth mechanism that is illustrated in Figure 5. We believe that the formation of flowerlike CZTS particles could be rationally expressed as a kinetically controlled nucleation−dissolution−recrystallization mechanism.[25] With the magnetic stirring, metal ions complexed with thiourea (Tu) in solution to form metal−Tu complexes. At the solvothermal temperature, Tu reacted with the trace water introduced by the solvent or hydrated metal salt and produces hydrogen sulfide (H_2S).[26] At the same time, the Cu−Tu complexes were thermally decomposed into Cu^{2+} ions and then reduced into Cu^{+} by the H_2S.[27] With the solvothermal process, Cu^{+}, Zn^{2+}, Sn^{4+}, and S^{2-} ions in the solution organized themselves to form the crystal nucleus spontaneously then the crystal growth follows. With the proceeding of the reaction, the tiny crystal nucleus grows up to particles with different sizes. Compared with small particles, the large ones have lower surface free energy. On the basis of the Ostwald ripening process, the large particles may grow up at the cost of the small ones.[28] At the same time, PVP was adsorbed on the particle surface to form the primary nanoparticles. The primary CZTS solid spheres are thermodynamically unstable due to the high energy on the surfaces of the particles, and there is an intrinsic tendency for partial CZTS nanoparticles to disperse and dissolve in the solution and further grow up to plateletlike nanoparticles through oriented aggregation.[25] After a long time reaction, the crystalline state of CZTS particles gradually changed from polycrystal to single crystal by the grain rotation induced grain coalescence (GRIGC) mechanism.[29] Finally, the

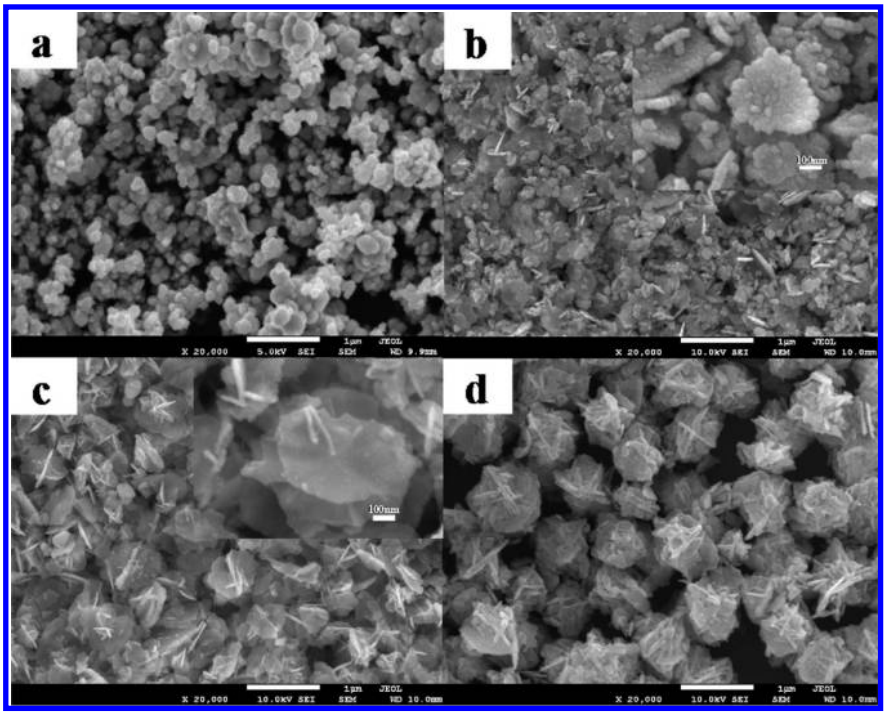

Figure 4. Time-dependent morphological evolution of the CZTS particles at different growth stages: a, 0.5 h; b, 2 h; c, 6 h; d, 24 h. The scale bar is 1 μm (the scale bar of the inset is 100 nm).

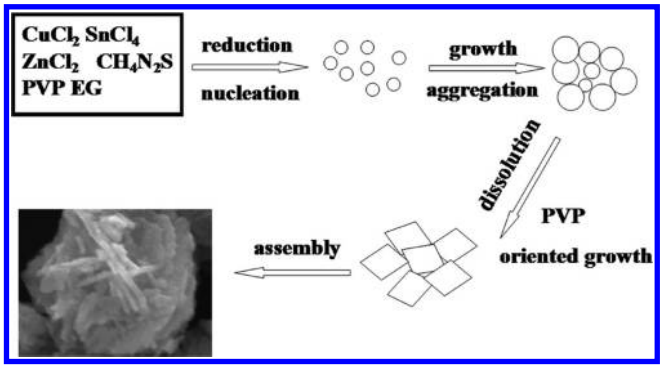

Figure 5. Schematic illustrations of the formation process for flowerlike CZTS particles assembled by nanosheets.

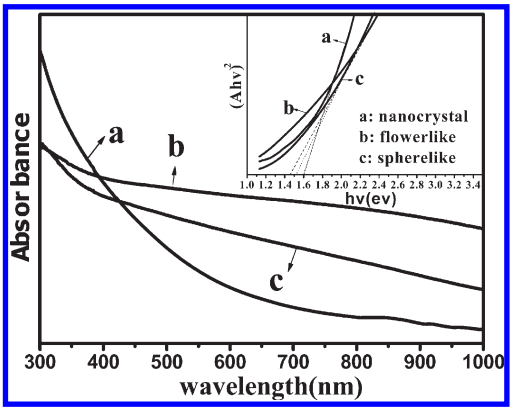

Figure 6. The UV−vis absorption spectra of the typical as-obtained CZTS particles. The inset shows the $(Ah\nu)^2$ vs $h\nu$ for the CZTS particles. The band gaps were estimated to be 1.47 eV (flowerlike nanoparticles), 1.52 eV (spherelike nanoparticles), and 1.60 eV (nanocrystals), respectively.

sheetlike nanoparticles gradually evolved to 3D hierarchical and flowerlike nanostructures through the self-assembly of sheetlike nanoparticles.

3.4. Optical and Electrical Properties. The absorption spectra were measured by the liquid phase method. The CZTS samples were dispersed in ethanol by ultrasound for several minutes, and then the final solution was transferred to the cuvette to measure the absorption spectra. The absorption spectra of the typical flowerlike particles, spherelike particles, and nanocrystals are shown in Figure 6. All the samples exhibited broad absorption in the visible region and the tails extended to longer wavelengths. We can see that the absorption of the flowerlike CZTS particles decayed more slowly than that of spherelike particles and nanocrystals. The difference of absorption may be caused by large surface area and light scattering, which were induced by the hierarchical structures. Compared to other CZTS materials (spherelike particles or nanocrystals), the flowerlike CZTS particles are considered as the best materials for the absorption layer in solar cells. The band gaps were obtained by plotting $(Ah\nu)^2$ as a function of $h\nu$ (A = absorbance, h = Planck's constant, and ν = frequency). From the long wavelength extrapolation of the band edge, the values of band gap for different kinds of nanoparticles were determined to be 1.47 eV (flowerlike particles), 1.53 eV (spherelike particles), and 1.60 eV (nanocrystals), respectively. As reported by Peng,[30] the band gap was found to be strongly dependent on the particle sizes of the products. In addition, the hierarchical structure may also affect the band gap of the products. The band gap value of flowerlike particles makes them the most suitable for the photovoltaic applications. To study the electrical properties of the CZTS particles, simple PV devices

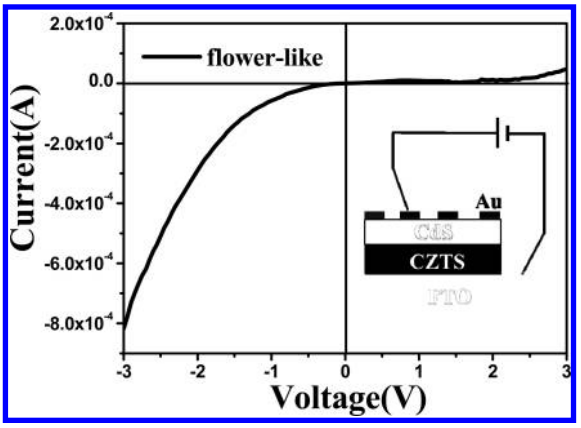

Figure 7. *I*−*V* curve of the film consisting of flowerlike CZTS particles. The inset shows the device structure used for electrical measurement.

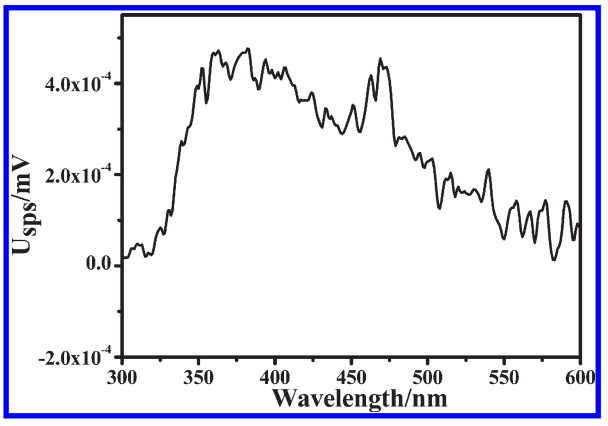

Figure 8. The surface photovoltage spectrum of CZTS film fabricated with flowerlike CZTS particles.

were fabricated with different kinds of CZTS particles. The device structure is shown in the inset of Figure 7. The fabrication details are as follows: The FTO glass was used as the substrate and was thoroughly washed with a mixed solution of deionized water, acetone, and 2-propanol (volume rations of 1:1:1) under sonication for 60 min before fabrication of CZTS films. CZTS films were fabricated on FTO glass by the knife coating method using a dense DDT solution of CZTS particles or nanocrystals. After coating, the CZTS films were vacuum-dried at 60 °C and then a postanneal process was conducted in an Ar atmosphere at a rate of 10 °C/min and held at 500 °C for 30 min. The buffer layer, cadmium sulfide (CdS), was deposited on CZTS films by the chemical bath method at 65 °C for 20 min and then annealed at 200 °C for 20 min. At last, the PV devices were completed by RF sputtering of Au electrode. The unannealed (a) and annealed (b) top view SEM images of the CZTS−FTO film are shown in Figure S8 (Supporting Information). We can see that the postannealed samples still kept the flowerlike status, and obvious particle growth of CZTS particles was not observed. The reason for this phenomenon may be explained by the large particle size of particles and short time of the annealing process. In addition, the presence of DDT may also affect the particle growth. The typical *I*−*V* curve of the CZTS film fabricated with flowerlike CZTS particles is shown in Figure 7. As shown in the Figure 7, the current increased sharply with the increase of reverse bias voltage, while the current increased slowly with the increase of forward bias voltage. This result indicated that the p−n heterojunction formed between the CZTS and CdS in the devices. The other devices fabricated with different kinds of CZTS particles (or nanocrystals) exhibited some rectifying characteristics (Figure S9, Supporting Information). In addition, the ratio of the electrical resistivity of CZTS films was estimated to be 1:20:75 (flowerlike particles:spherelike particles: nanocrystals). The difference of current−voltage characteristics between the three devices may come from the difference of the morphologies and sizes of CZTS particles (or nanocrystals). On the basis of the above analysis, we believe that the flowerlike CZTS particles are favorable to increase of current carrier concentration and electron transmission. The surface photovoltage technique is an effectively way to study the process of photoinduced charge separation and transfer in the surface and interface. The surface photovoltage spectrum of the typical flowerlike CZTS film showed significant surface photovoltage effect between 300 and 600 nm (see Figure 8). This result indicated the potential of photocurrent generation and thus the great potential use of hierarchical CZTS particles in solar cells.

4. CONCLUSION

In conclusion, the hierarchical nanostructures including flowerlike CZTS particles and spherelike particles have been prepared by changing the reaction conditions via the convenient solvothermal method. The XRD, EDS, TEM, SEM, SAED, Raman spectrum, and EDS mapping characterizations confirmed the structure, composition, and morphology of the as-obtained particles. The nucleation−dissolution−recrystallization mechanism was proposed for the organization of the flowerlike CZTS nanostructures. Different synthetic conditions such as reaction temperature, reaction time, concentration, and the amount of PVP can influence and control the size and morphology of the products. The UV−vis absorption spectra revealed that the typical flowerlike CZTS particles have strong optical absorption in the visible region compared with the spherelike particles and nanocrystals, and the band gap matches well with that of the bulk CZTS materials. Meanwhile, the *I*−*V* curve and the surface photovoltage spectrum showed that the hierarchical structure favored generation of photoinduced carrier and electronic transmission. The surface photovoltage spectrum showed that the hierarchical structure favored generation of photoinduced carrier and electronic transmission. We believe that this hierarchical nanostructure with special advantages has potential use in photovoltaic devices.

■ ASSOCIATED CONTENT

Supporting Information. Figures S1−S9 and Table S1. This material is available free of charge via the Internet at http://pubs.acs.org.

■ AUTHOR INFORMATION

Corresponding Author

*E-mail: zhouwh@henu.edu.cn (W.-H.Z.), wusixin@henu.edu.cn (S.-X.W.).

■ ACKNOWLEDGMENT

This project is supported by the National Natural Science Foundation of China (20871041and 20903033), the New Century

Excellent Talents in University (NCET-08-0659), the Doctoral Scientific Research Foundation of Henan University (B2010079), and the Scientific Research Foundation of Henan University (2010YBZR014).

REFERENCES

(1) Ito, K.; Nakazawa, T. *Jpn. J. Appl. Phys.* **1988**, *27*, 2094–2097.
(2) Jackson, P.; Hariskos, D.; Lotter, E.; Paetel, S. *Prog. Photovoltaics: Res. Appl.* DOI: 10.1002/pip.1078.
(3) Scragg, J. J.; Dale, P. J.; Peter, L. M.; Zoppi, G.; Forbes, I. *Phys. Stat. Sol. B* **2008**, *245*, 1772–1778.
(4) Kameyama, T.; Osaki, T.; Okazaki, K.; Shibayama, T.; Kudo, A.; Kuwabata, S.; Torimoto, T. *J. Mater. Chem.* **2010**, *20*, 5319–5324.
(5) Katagiri, H. *Thin Solid Films* **2005**, *480*−*481*, 426–432.
(6) Katagiri, H.; Jimbo, K.; Yamada, S.; Kamimura, T.; Maw, W. S.; Fukano, T.; Ito, T.; Motohiro, T. *Appl. Phys. Express* **2008**, *1*, 041201.
(7) Nakayama, N.; Ito, K. *Appl. Surf. Sci.* **1996**, *92*, 171–175.
(8) Katagiri, H.; Jimbo, K.; Maw, W. S.; Oishi, K.; Yamazaki, M.; Araki, H.; Takeuchi, A. *Thin Solid Films* **2009**, *517*, 2455–2460.
(9) Guo, Q.; Hillhouse, H. W.; Agrawal, R. *J. Am. Chem. Soc.* **2009**, *131*, 11672–11673.
(10) Riha, S. C.; Parkinson, B. A.; Prieto, A. L. *J. Am. Chem. Soc.* **2009**, *131*, 12054–12055.
(11) Steinhagen, C.; Panthani, M. G.; Akhavan, V.; Goodfellow, B.; Koo, B.; Korgel, B. A. *J. Am. Chem. Soc.* **2009**, *131*, 12554–12555.
(12) Guo, Q.; Ford, G. M.; Yang, W. C.; Walker, B. C.; Stach, E. A.; Hillhouse, H. W.; Agrawal, R. *J. Am. Chem. Soc.* **2010**, *132*, 17384–17386.
(13) Zou, C.; Zhang, L. J.; Lin, D. S.; Yang, Y.; Li, Q.; Xu, X. J.; Chen, X. A.; Huang, S. M. *CrystEngComm* **2011**, *13*, 3310–3313.
(14) Todorov, T. K.; Reuter, K. B.; Mitzi, D. B. *Adv. Mater.* **2010**, *22*, E156–E159.
(15) Yoo, H.; Kim, J. H. *Sol. Energy Mater. Sol. Cells* **2011**, *95*, 239–244.
(16) Susanne, S. *Sol. Energy Mater. Sol. Cells* **2011**, *95*, 1471–1476.
(17) Alivisatos, A. P. *Science* **1996**, *271*, 933–937.
(18) Zhong, L. S.; Hu, J. S.; Liang, H. P.; Cao, A. M.; Song, W. G.; Wan, L. J. *Adv. Mater.* **2006**, *18*, 2426–2431.
(19) Bierman, M. J.; Jin, S. *Energy Environ. Sci.* **2009**, *2*, 1050–1059.
(20) Zhang, Q. F.; Cao, G. Z. *J. Mater. Chem.* **2011**, *21*, 6769–6774.
(21) Grossberg, M.; Krustok, J.; Raudoja, J.; Timmo, K.; Altosaar, M.; Raadik, T. *Thin Solid Films* **2011**, *519*, 7403–7406.
(22) Wang, Q. Q.; Zhao, G. L.; Han, G. R. *Mater. Lett.* **2005**, *59*, 2625–2629.
(23) Si, R.; Zhang, Y. W.; You, L. P.; Yan, C. H. *Angew. Chem., Int. Ed.* **2005**, *44*, 3256–3260.
(24) Zhang, Y. J.; Yao, Q.; Zhang, Y.; Cui, T. Y.; Li, D.; Liu, W.; Lawrence, W.; Zhang, Z. D. *Cryst. Growth Des.* **2008**, *8*, 3206–3212.
(25) Luo, Y. S.; Zhang, W. D.; Dai, X. J.; Yang, Y.; Fu, S. Y. *J. Phys. Chem. C* **2009**, *113*, 4856–4861.
(26) Yu, S. H.; Shu, L.; Yang, J.; Han, Z. H.; Qian, Y. T.; Zhang, Y. H. *J. Mater. Res.* **1999**, *14*, 4157–4162.
(27) Han, S. K.; Kong, M. G.; Guo, Y.; Wang, M. T. *Mater. Lett.* **2009**, *63*, 1192–1194.
(28) Roosen, A. R.; Carter, W. C. *Physica A* **1998**, *261*, 232–247.
(29) Moldovan, D.; Yamakov, V.; Wolf, D.; Phillpot, S. R. *Phys. Rev. Lett.* **2002**, *89*, 206101.
(30) Xie, R. G.; Rutherford, M.; Peng, X. G. *J. Am. Chem. Soc.* **2009**, *131*, 5691–5697.